

## Article

# High-Temperature Oxidation of CrN/ZrN Multilayer Coatings

Andrey Vorontsov <sup>1,\*</sup>, Andrey Filippov <sup>1,\*</sup>, Nickolay Shamarin <sup>1</sup>, Evgeny Moskvichev <sup>1</sup>, Olga Novitskaya <sup>1</sup>, Evgenii Knyazhev <sup>1</sup>, Yuliya Denisova <sup>2</sup>, Andrei Leonov <sup>2</sup>, Vladimir Denisov <sup>2</sup> and Sergei Tarasov <sup>1</sup>

<sup>1</sup> Institute of Strength Physics and Materials Sciences, Siberian Branch of Russian Academy of Sciences, Per. Academicheskii 2/4, 634055 Tomsk, Russia

<sup>2</sup> Institute of High Current Electronics, Siberian Branch of Russian Academy of Sciences, Per. Academicheskii 2/3, 634055 Tomsk, Russia

\* Correspondence: vav@ispms.ru (A.V.); avf@ispms.ru (A.F.)

**Abstract:** Multilayer nitride coatings provide some of the best performance when in their use for the production of metalworking tools. In this work, vacuum-arc plasma-assisted deposited multilayer ZrN/CrN coatings with different numbers of constituent layers were characterized for high-temperature oxidization in air using weighing, confocal and scanning electron microscopy and synchrotron XRD. Oxidizing at 300 °C did not deteriorate the coating surfaces, while higher temperatures caused surface deterioration and oxidation accompanied by cracking, delamination and considerable mass gains. The coating with higher number of thinner layers showed higher oxidation resistance due to more prominent oxygen barrier effect.

**Keywords:** nitrides coating; X-ray analysis; phase composition; high temperature; oxidation; diffusion



**Citation:** Vorontsov, A.; Filippov, A.; Shamarin, N.; Moskvichev, E.; Novitskaya, O.; Knyazhev, E.; Denisova, Y.; Leonov, A.; Denisov, V.; Tarasov, S. High-Temperature Oxidation of CrN/ZrN Multilayer Coatings. *Metals* **2022**, *12*, 1746. <https://doi.org/10.3390/met12101746>

Academic Editor: Yongho Sohn

Received: 3 September 2022

Accepted: 11 October 2022

Published: 17 October 2022

**Publisher's Note:** MDPI stays neutral with regard to jurisdictional claims in published maps and institutional affiliations.



**Copyright:** © 2022 by the authors. Licensee MDPI, Basel, Switzerland. This article is an open access article distributed under the terms and conditions of the Creative Commons Attribution (CC BY) license (<https://creativecommons.org/licenses/by/4.0/>).

## 1. Introduction

Corrosion protection and wear-resistant coatings are widely used in various mechanical industries for improving service characteristics and reducing the exploitation costs of metal processing, forming tools, and equipment and engine component production. These coatings are made of nitrides of metals such as chromium, niobium, tantalum, titanium, as well as their combinations [1–3].

There are many methods used for deposition of nitride coatings, such as reactive magnetron sputtering [2,4], vacuum brazing [4], thermal spraying [5], CVD, pulse electrodeposition [6], as well as the PVD vacuum-arc plasma-assisted deposition [7] that has been used in our work. Despite their widespread application for improving characteristics of metal cutting tools, the nitride coatings are still the subject of investigations with respect to tailoring their composition, microstructures and mechanical properties for more intense working conditions. The greatest concern is their corrosion resistance [8] and high-temperature oxidation [4,9]. For instance, multilayer Cr/CrN coatings deposited on a zirconium alloy substrate demonstrated improved resistance to hot steam corrosion, with decreasing in the constituent layer thickness [8]. Such an improvement was related to oxidizing the zirconium and formation of a dense uniform layer of zirconia that served as a barrier against oxygen penetration inside the zirconium alloy.

Other research efforts were focused on studying reactive magnetron-sputtered Cr-Zr-N-O coatings [10–12]. Such an approach can be used to improve the mechanical characteristics of the coatings, in particular fracture toughness, by forming oxynitride solid solutions.

Spitz et al. [10] deposited Cr-Zr-N-O thin films with different component concentrations and characterized them for mechanical characteristics. The Young modulus reduction was the results of forming more nitrides instead of oxides.

Thermal stability of (Cr,Zr)<sub>2</sub>O<sub>3</sub> films was studied by Landälv et al. [11], who discovered formation of α-(Cr,Zr)<sub>2</sub>O<sub>3</sub> and amorphous (Zr,Cr)O<sub>x</sub> phases in as-deposited coatings.

Mohammadtaheri et al. reported on forming  $t\text{-ZrO}_2 + m\text{-ZrO}_2 + h\text{-Cr}_2\text{O}_3(\text{Cr,Zr})_2\text{O}_3$  after high-temperature oxidization of Cr-Zr-O films [12]. Thermal stability of these coatings was higher than that of chromium oxide ones because of their Zr solubility. Therefore, deposition of complex Cr-Zr-N-O coatings may allow the improvement of both the mechanical characteristics and the thermal stability of the coatings. High-temperature oxidation of deposited CrN/ZrN multilayer coatings may allow obtaining such an effect due to forming mixed Cr and Zr oxides.

In connection with this, the objective of this work is to study phase composition and evolution of multilayer CrN/ZrN coatings deposited on a WC-Co substrates during high-temperature oxidation.

## 2. Materials and Methods

The multilayer CrN/ZrN coatings were obtained by means of vacuum-arc plasma-assisted deposition on WC-8 wt.% Co substrates using the QUINTA facility (HCEI SB RAS, Tomsk, Russia) [13]. The substrates were secured on a planetary rotating table with sample holder whose rotation rate was in direct proportion to that of the table.

The substrate pre-heating to 400 °C was performed by igniting the gas discharge with 40 A current and applying the 700 V bias voltage. Ion bombardment was used to clean the substrate surfaces, with the ensuing filling the chamber with nitrogen/argon gas mixture (90/10) up to required pressure level and igniting of the 80 A discharge on each of the two evaporators (HCEI SB RAS, Tomsk, Russia). The evaporators contained cathodes made of either 99.5%—pure Zr or 99.9%—pure Cr. Two different rotation rates were chosen for the table such as 0.5 RPM and 8 RPM, which corresponded to the substrate rotation rates 20, and 320 RPM, respectively.

The coatings obtained using 0.5 RPM or 8 RPM rotation rates were composed of different number of layers (Figure 1). The layer thickness (Figure 1c,d) was 5.43 nm and 3.2 nm (based on TEM results) for the sample deposited at 0.5 rpm (Figure 1a,c) and 8 rpm (Figure 1b,d), respectively. In SEM analysis only the macro layers (61.9 nm, Figure 1c) for the sample deposited at 0.5 rpm can be determined (Figure 1a), whereas for the sample deposited at 8 rpm no coating layers are observable at this resolution (Figure 1b). The macrolayer periodical contrast is related to periodic oscillations of both Zr and Cr concentrations occurred in the coating during 0.5 RPM deposition because of planetary rotation scheme specifics [14]. Despite containing different numbers of ZrN and CrN layers both multilayer coatings had the same 5 µm thicknesses.

The as-deposited coating was subjected to oxidization in air at temperatures 300, 600, 700, and 900 °C for 15 min and then investigated using confocal microscope Olympus (Olympus Corporation, Shinjuku, Japan), SEM instrument Apreo 2S (Thermo Fisher Scientific, Waltham, MA, USA), synchrotron XRD (BINP SB RAS, Novosibirsk, Russia) (Synchrotron X-ray Source VEPP-3, wavelength 1.54 Å) and weighing for detecting their mass gains. The oxidation temperature 700 °C was chosen as an intermediate temperature to carry out the oxidized surface analysis instead of that oxidized at 900 °C, which was totally deteriorated and not available for SEM studies. The weighing of each sample before and after was carried out using an analytical balance machine CP124 S (Sartorius, Goettingen, Germany) to accuracy of 0.0001. Phases in the samples were identified using Match! 3 software (version 3.1, Crystal impact, Kreuzherrenstraße, Germany) and PDF database.

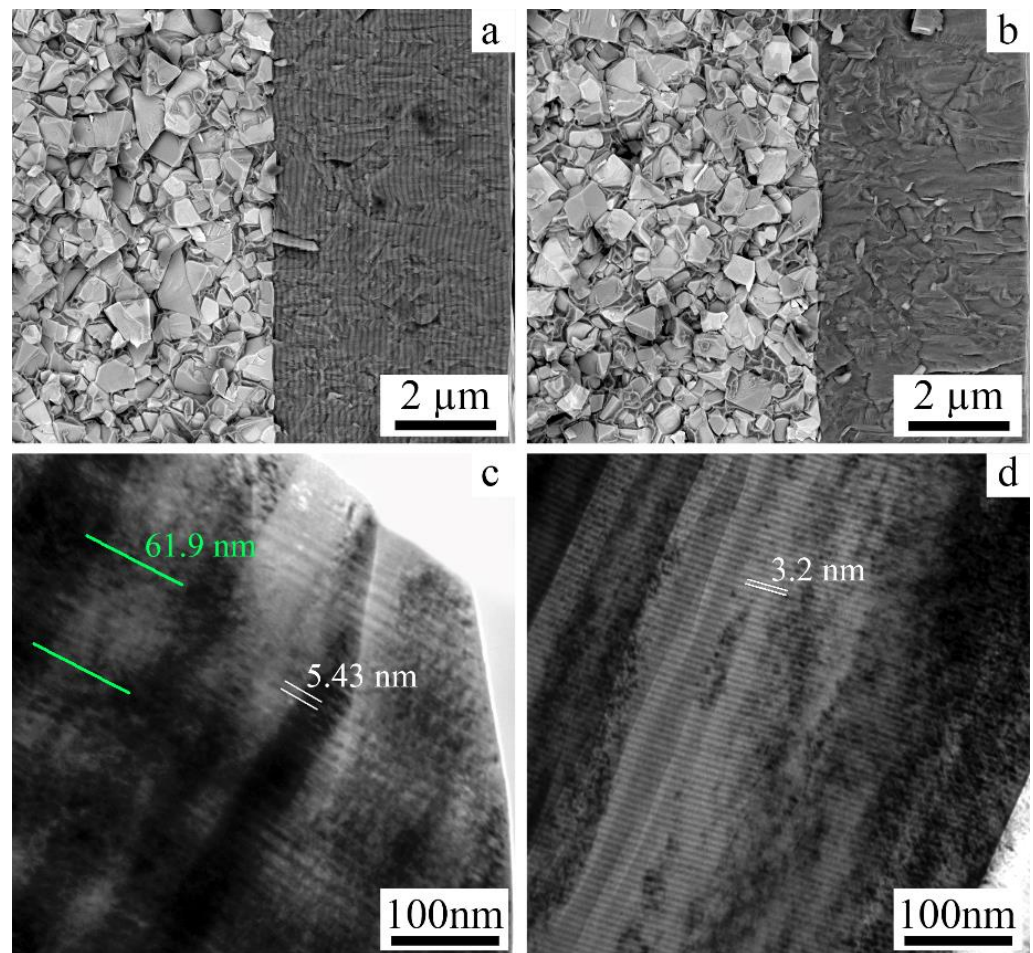


**Figure 1.** SEM (a,b) and TEM (c,d) cross-section views of the 0.5 RPM (a,c) and 8 RPM (b,d) multilayer coatings.

### 3. Results

#### 3.1. Mass Change of Coatings after Oxidation

High-temperature oxidization is accompanied by increasing the mass of the sample, and therefore weighing is one of the method to study oxidization kinetics at different temperatures. The results of weighing the multilayer coating samples were represented as the differences of masses before and after the oxidization related to the corresponding coating surface areas (Figure 2). It was found out that the mass gain dependence on the oxidization temperature was almost the same for both coating deposition regimes.

The use of a logarithmic scale axis was a convenient way to represent the results of weighing, owing to the too great a difference ( $\Delta m$ ) between the mass gains achieved at different oxidization temperatures. For example, oxidization at temperatures 300, 600, and 700 °C resulted in mass gains  $1.8222 \pm 0.0387$  mg/cm<sup>2</sup>,  $3.5342 \pm 0.1074$  mg/cm<sup>2</sup>, and  $11.5598 \pm 0.3510$  mg/cm<sup>2</sup>, respectively, i.e., about orders of magnitude lower than that of for 900 °C which amounted up to  $534.4559 \pm 56.8185$  mg/cm<sup>2</sup>.

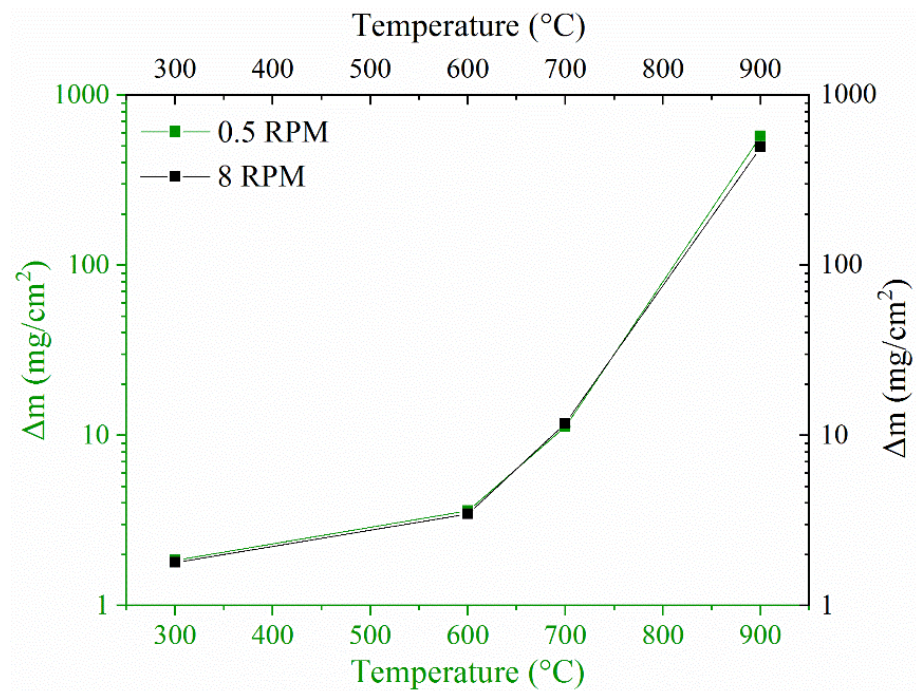


**Figure 2.** The mass gains due to oxidation for samples obtained using 0.5 RPM and 8 RPM deposition regimes.

### 3.2. Surface Roughness of Coatings after Oxidation

Oxidized surfaces of the coatings were examined using a confocal microscopy that allowed reproducing the oxidized surface 3D roughness (Figure 3) as well as roughness characteristics (Figure 4). The coating surfaces oxidized at 300 °C are shown in Figure 3a,d where color gradation scales correspond to maximum asperity height 7 μm. The same asperity height scale and surface roughness was obtained also for both as-deposited coatings, which are not shown here for brevity reasons. Also there is no difference in surface topology between Figure 3a,d that represent different deposition regimes. Numerical characteristics of roughness obtained from 70 × 70 μm central areas of corresponding confocal images clearly show the differences among the samples (Figure 4). Both surfaces oxidized at 300 °C demonstrate roughness as low as 83.5 ± 3.4 nm, the same as the as-deposited coatings. Therefore, both coatings showed good resistance to oxidation at 300 °C.

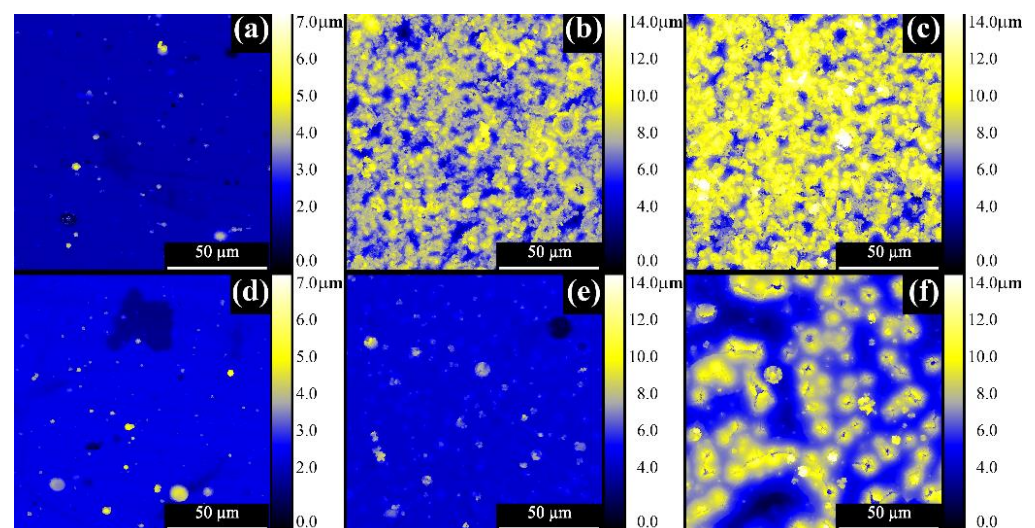


**Figure 3.** The multilayer coating surfaces oxidized at 300 °C (a,d), 600 °C (b,e) and 700 °C (c,f).

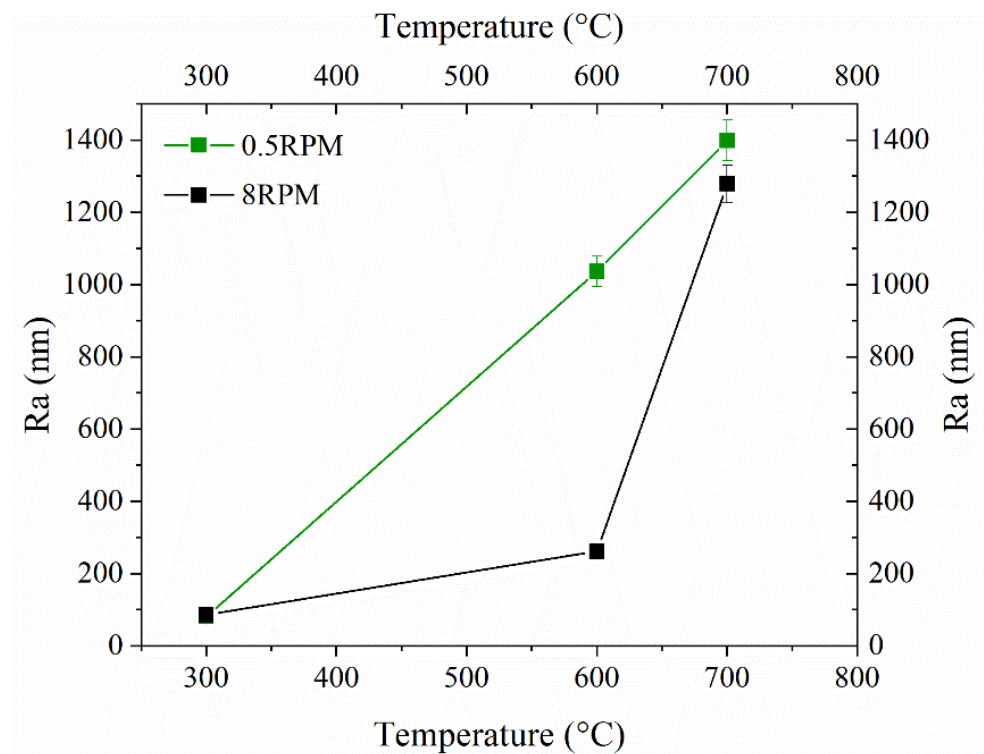


**Figure 4.** Roughness of the multilayer coatings oxidized at different temperatures.

The multilayer coating deposited at 0.5 RPM rotation (Figure 3a–c) and then oxidized at 600 °C for 15 min demonstrate an almost totally rough oxidized surface in Figure 3b as compared to that obtained at 8 RPM (Figure 3e) which looks as almost the same as that in Figure 3c. The 0.5 RPM (Figure 3b) and 8 RPM (Figure 3e) oxidized coatings demonstrated roughness's 1  $\mu\text{m}$  and 262 nm, respectively (Figure 4). It seems that the coating deposited at 8 RPM rotation demonstrated more resistance with respect to medium temperature oxidation as compared to that of deposited at low rotation rate of 0.5 RPM.

Coating obtained at 0.5 RPM and then oxidized at 700 °C (Figure 3c) reveals a totally deteriorated area of the sample with even more rough surfaces, while that of the sample obtained at 8 RPM shows cracking and delamination regions (Figure 3f). Both surfaces, however, show the Ra roughness in the order of 1.2  $\mu\text{m}$ , i.e., 24% of the total coating thickness (Figure 4). Again, the 8 RPM coating showed higher resistance to oxidation as compared to that obtained at 0.5 RPM. However, the difference was not as high as for oxidation at 600 °C. The loss of oxidation resistance of the 8 RPM sample started from 600 °C and at 700 °C, and became almost the same as that of 0.5 RPM. Coatings exposed to oxidation at 900 °C revealed their completely deteriorated surfaces that did not allow describing the surface roughness and surface morphology.

The roughness profiling in Figure 5 allows for observing the difference in the asperity and trough distributions as measured on all the oxidized samples. The 0.5 RPM sample can be characterized by a lower space period waviness than that of the 8 RPM sample, at almost equal asperity heights (Figure 5).

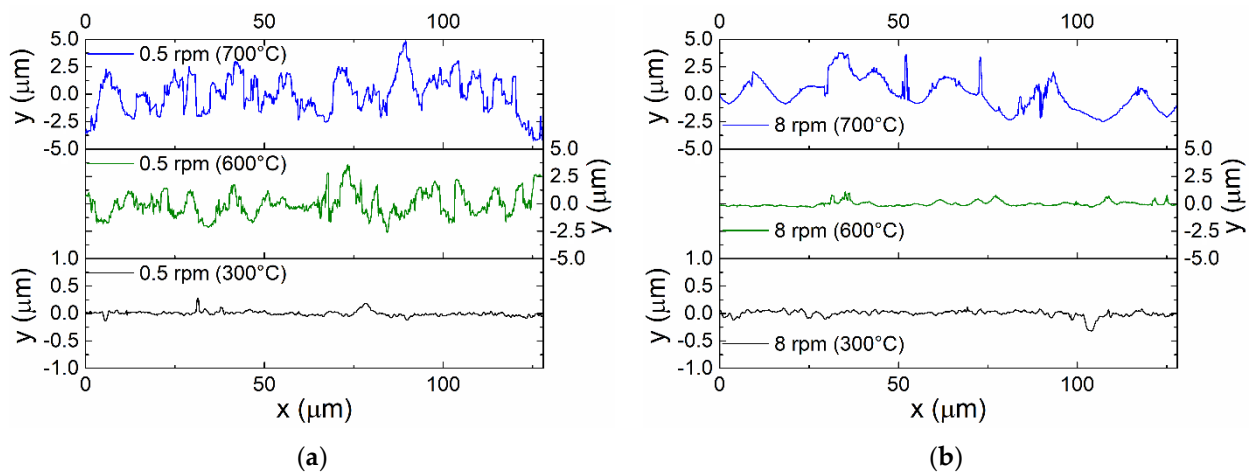


**Figure 5.** Roughness profiles obtained from oxidized surfaces of multilayer coatings deposited at 0.5 (a) and 8 RPM (b) rotation rates.

### 3.3. Oxidized Surface Morphology

Thorough examinations of both types of multilayer coatings oxidized at 300, 600, and 700 °C were carried out using SEM (Figure 6). The first type of coatings was deposited at 0.5 RPN rotation. Morphologically, the surfaces oxidized at 300 °C were similar and represented by as-deposited layer with isolated oxidized blisters. It could be seen that both number and size of these blisters are higher in case of the 0.5 RPM coating (Figure 6a) as compared to those on the 8 RPM one (Figure 6d). Such a morphological difference becomes absolutely clear when comparing the surfaces oxidized at 600 °C. The 0.5 RPM coating is represented by totally deteriorated surface with large dimples, craters, pits and cracks (Figure 6b), while that of 8 RPM is still rather smooth with isolated growing and cracked blisters (Figure 6e). The 0.5 RPM coating oxidized at 700 °C differs from that obtained at 600 °C by the presence of larger dimples, pits and cracks (Figure 6c). The 8 RPM surface looks less deteriorated with small oxidized and large cracked blisters as well as crevices, but still shows some non-oxidized regions (Figure 6f).

EDS element concentration differences as obtained from all the oxidized surfaces shown in Figure 6 proved to be within the EDS method errors (Figure 7). Concentrations of the substrate elements such as W and Co were less than 0.5 at.% with maximum at 0.31 at.% in the 0.5 RPM sample. Qualitatively it can be observed from Figure 7a,b that oxygen concentration increased greatly on the coatings oxidized at 600 °C with ensuing moderate growth at 700 °C.

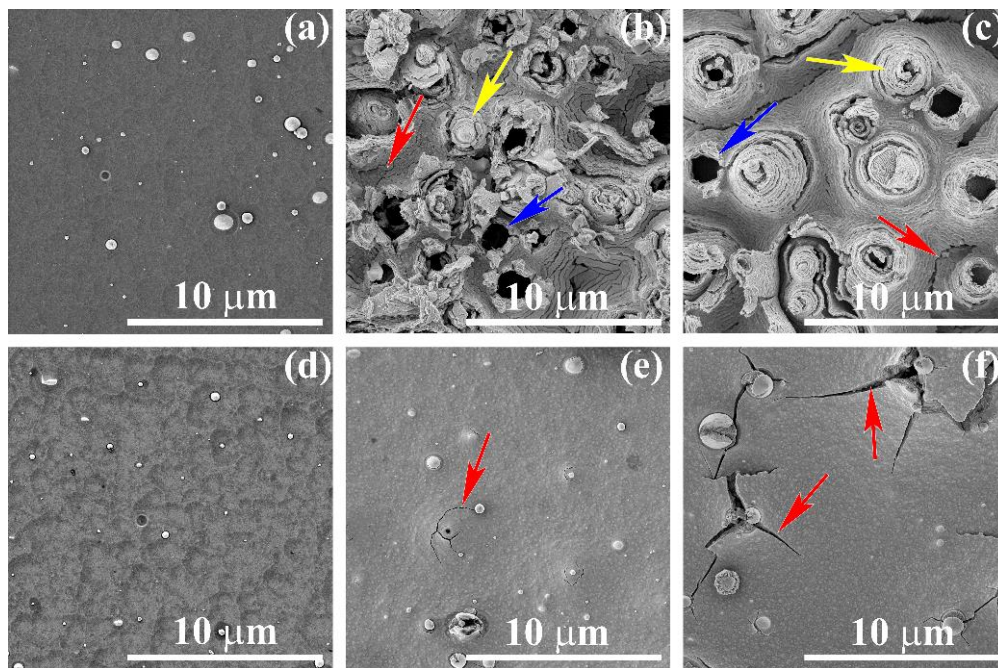


**Figure 6.** SEM SE images of 0.5 RPM (a–c) and 8 RPM (d–f) multilayer coatings oxidized at 300 (a,d), 600 (b,e) and 700 °C (c,f). Yellow, blue and red arrows denote cracked blisters, craters and cracks, respectively.

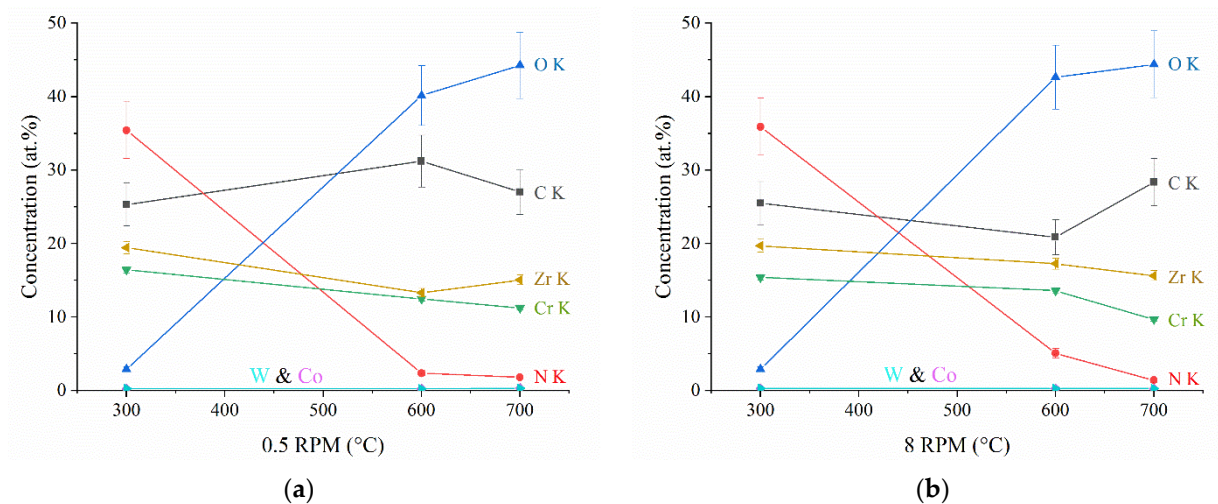


**Figure 7.** EDS element concentrations on 0.5 RPM (a) and 8 RPM (b) multilayer coatings oxidized at 300, 600 and 700 °C.

### 3.4. Phase Identification Using Synchrotrone XRD

Phase and chemical evolution of the coatings that would occur during high-temperature oxidation has been studied using the XRD with synchrotron radiation. The as-deposited multilayer coatings allowed identifying phases such as CrN, ZrN,  $\beta$ -Zr and WC (Figure 8a,b). The presence of the WC peaks is explained by diffraction from the WC-grains in the substrate underneath the coatings after full penetration of X-rays through the coating.

The diffractograms obtained from coatings oxidized at 300, 600, 700 and 900 °C demonstrated the presence of phases such as Zr, ZrO<sub>2</sub>, ZrC, Cr<sub>2</sub>O<sub>3</sub>, C<sub>23</sub>C<sub>6</sub> and WC (Figure 8a,b).

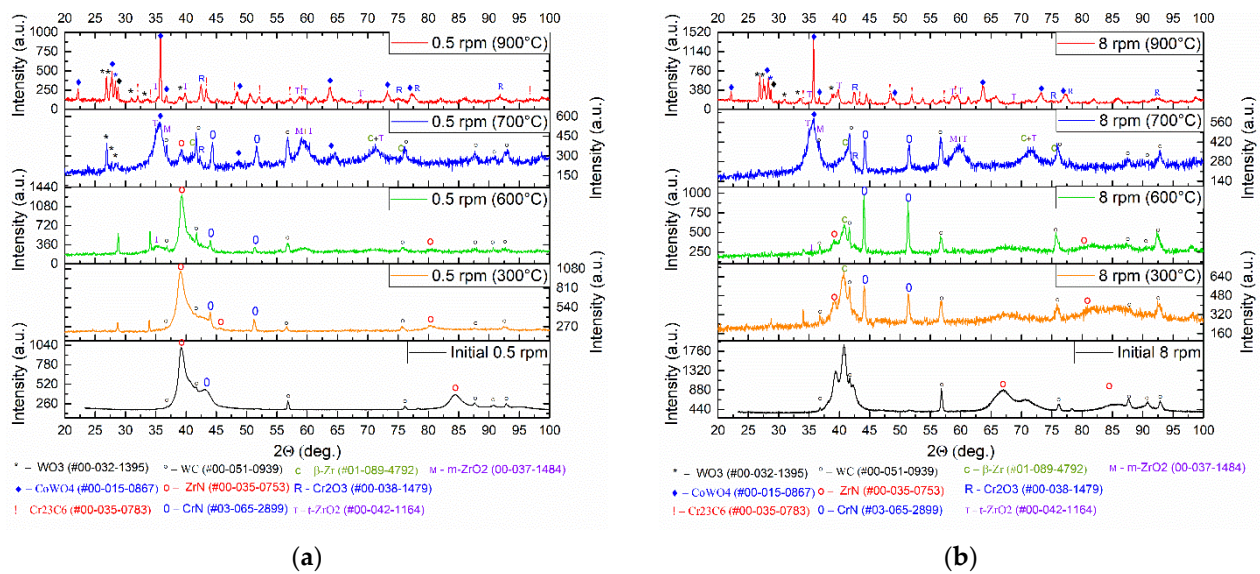


**Figure 8.** The diffractograms obtained from the surfaces of as-deposited and oxidized at 300, 600, 700 and 900 °C 0.5 RPM (a) and 8 RPM (b) coatings.

Both coatings are made of contain CrN and ZrN phases that, being heated in air to 300 °C, allow for identifying the presence of both  $\text{Cr}_2\text{O}_3$  and monoclinic  $m\text{-ZrO}_2$  whose highest peaks can be observed at  $2\theta \leq 35^\circ$ . At the same time there are  $(111)_{\text{CrN}}$  and  $(200)_{\text{CrN}}$  as well as  $(002)_{\alpha\text{-Zr}}$  reflections in both types of the coatings. However, their presence is most clear in the 8 RPM sample, whose oxidation resistance is higher judging by the above-discussed results.

Oxidizing the 0.5 RPM sample at 600 °C resulted in  $m\text{-ZrO}_2 \rightarrow t\text{-ZrO}_2$  transformation of monoclinic zirconia into its tetragonal phase. No such transformation occurred in the 8 RPM sample or the amount of  $\text{ZrO}_2$  was below the XRD method sensitivity. Instead, this sample still contains much of the CrN.

Increasing the oxidizing temperature to 700 °C caused  $m\text{-ZrO}_2 \rightarrow t\text{-ZrO}_2$  transformation in both types of coating, as detected by growing heights of the  $t\text{-ZrO}_2$  (101), (112) and (200) peaks and corresponding decreasing of the ZrN peak heights. In distinction to ZrN, the CrN phase content retained with the temperature. In addition, the oxidized-at-700 °C surface of the 0.5 RPM sample revealed (002), (020) and (200) peaks belonging to the tungsten trioxide  $\text{WO}_3$ .

Testing at 900 °C caused almost full deterioration of the sample surfaces with corresponding intense delamination and spalling due to volume expansion during  $\text{ZrN} \rightarrow m\text{-ZrO}_2$  reaction on both samples. Their XRD patterns were practically the same as those obtained at 700 °C with additional phases such as monoclinic  $\text{WO}_3$  and  $\text{CoWO}_4$ , ZrC as well as  $\text{M}_{23}\text{C}_6$ , where M stands for Cr and W.

#### 4. Discussion

The results obtained in this work allow for understanding the phase evolution of the multilayer ZrN/CrN coatings under condition of high-temperature oxidization in air. However, the reasons behind coating formation mechanism dependence from the deposition parameters are still unclear. Our previous investigation [14] was devoted to studying macro- and microstructural characteristics of the multilayer coatings deposited using different deposition process regimes. This time, the choice was to use minimal and maximal sample rotation rates for a better understanding of the effect of different CrN/ZrN interlayer thickness and the growth texturing on their behaviors under high-temperature air conditions.

The weighing showed that high-temperature heating in air did not result in the different behaviors of both types of coating, but only indicated on the fact that heating to 600–700 °C caused sharp rise of the samples' masses. Since no extra matter except for that of oxygen was added during the oxidation, the mass gain effect may be fully related to oxidizing the coating components. However, when looking at the results of both XRD and SEM, one can notice the presence of heavy elements such as W and Co as well as C on the surfaces oxidized at temperatures > 700 °C. Since these elements are components of the WC–Co substrate, it can be suggested that high-temperature heating caused oxidation of Co and WC according to reactions (1) and (2) as follows:



Then  $\text{CoWO}_4$  may result from reaction between cobalt and tungsten oxides:



These W and Co oxides contain more oxygen in the oxidized coating, as compared to that of  $\text{ZrO}_2$ , and therefore allow additional mass gain at high temperatures.

It is known that CO is an efficient reducing agent and therefore might reduce the oxides already formed in the coating. In particular, it might have reduced the chromium oxide and even form then a chromium–base carbide  $\text{M}_{23}\text{C}_6$ .

When ZrN is oxidized according epitaxial growth of t- $\text{ZrO}_2$ , there could be tensile stress and even cracks on the  $\text{ZrO}_2$ -ZrN interfaces that facilitate t- $\text{ZrO}_2 \rightarrow$  m- $\text{ZrO}_2$  transformation [15,16] so that final product will be from the monoclinic phase.

However, it was found that starting from 600 °C, the tetragonal phase was detected in the 0.5RPM coating. Such a finding means that tetragonal phase was stabilized due to some factor such as nanometer crystallite size, internal compression stress, and/or doping elements with lower valences that cause formation of oxygen vacancies especially at high temperatures [17]. It could be noted that the as-deposited 0.5RPM and 8RPM coatings are characterized by the presence of residual stresses about  $-8.25$  MPa and 839 MPa, respectively [14], which could have an effect on the phase equilibrium during oxidation. From this point of view, the tetragonal phase might have been stabilized by residual compression stress that suppress the t- $\text{ZrO}_2 \rightarrow$  m- $\text{ZrO}_2$  transformation in the 0.5 RPM coating, oxidized at 600 °C. These stresses are generated depending upon the deposition process parameters and heating/cooling process [18].

CO is a reducing agent that may cause partial reduction of the  $\text{ZrO}_2$  and formation of oxygen vacancies [19]. The presence of metallic  $\beta$ -Zr in both coatings may be the result of such a reduction. Better diffusion of oxygen through the 0.5 RPM layers might cause earlier oxidation of the WC-Co substrate and a release of reducing CO agent as compared to that in the less penetrable 8 RPM sample. Considerations like these may help explain the t- $\text{ZrO}_2$  that stabilization occurred in 0.5 RPM and 8 RPM samples at 600 °C and 700 °C, respectively.

It was shown above by the 8 RPM sample as it demonstrated higher oxidation resistance compared to that of the 0.5 RPM sample. However, it was reported [20] that almost the same blister type of surface deterioration was observed on a ZrN coating heated to 500 °C. The molar volumes of ZrN and m- $\text{ZrO}_2$  are 14.4 and 21.0  $\text{cm}^3 \text{ mol}^{-1}$  [16] and therefore stresses appear by means of dilatation effect in chemical reaction [20]



CrN oxidization at high temperatures includes several stages, with the first stage being the thermal decomposition of CrN into  $\text{Cr}_2\text{N}$  and the release of nitrogen atoms that produce vacancies then occupied by oxygen with ensuing formation of chromium oxide [8]. Also it was reported [21] that CrN has higher oxidation resistance as compared

to that of ZrN. Such a difference resulted in the fact that the CrN volume fraction grows with the oxidization temperature due to preferable oxidization of the ZrN. The multilayer coating with alternating ZrN/CrN layers would also possess lower oxidation resistance as compared to that made of pure CrN and ZrN [22]. In addition, the XRD analysis did not allow detecting any mixed Cr and Zr phases that might improve the thermal stability of the coatings. However, it does not mean that no such phases were formed both during deposition and oxidation between the successively deposited layers. It would be obvious that if formed between the layers these phases had more thermal stabilization effect in the 8 RPM coating as compared to that of 0.5 RPM.

However, the number and thickness of the layers composing the coating would play an important role too. Earlier it was demonstrated [14] that 0.5 RPM coating contains layers wider than those of the 8 RPM sample, i.e., for comparison 5.43 and 3.2 nm, respectively, at the same total coating thickness. In other words, the 8 RPM sample contains higher numbers of CrN layers which serve as effective barriers against the oxygen diffusion [9] and, thus attain improved oxidation resistance to the 8 RPM sample. Such a finding has important practical meaning for depositing anti-corrosion multilayer coatings with thicknesses less than 4  $\mu\text{m}$ .

## 5. Conclusions

Multilayer ZrN/CrN coatings intended for metal processing tools were deposited on WC–8 wt.% Co substrates using different deposition rates and then subjected to oxidization in air at temperatures 300, 600, 700, and 900 °C.

- Oxidization at 300 °C resulted in formation of isolated oxide blisters oxides on both types of coatings characterized by minor mass gains irrespective of the constituting layer thicknesses. Starting from 700 °C there was sharp growth of the sample masses with intense deterioration of the oxidized surfaces.
- The oxidation resistance of multilayer coatings depends on the number of constituent alternating CrN/ZrN layers which serve as barriers against oxygen diffusion inside the coating. From this point of view, the multilayer coating deposited using the fast sample rotation at 8 RPM proved to be more effective protection against oxidization at all temperatures used.
- High-temperature experiments showed that WC-Co substrate is subjected to oxidization by oxygen diffusion through the deteriorated coating with formation of tungsten trioxide and cobalt tungstate. The volatile product of WC oxidation is CO which may reduce the  $\text{Cr}_2\text{O}_3$  to Cr and even form  $\text{M}_{23}\text{C}_6$  carbides.
- Temperature-induced transformation  $m\text{-ZrO}_2 \rightarrow t\text{-ZrO}_2$  was observed at 600 °C on the 0.5 RPM coating with thick layers while 8 RPM thin layered coating contained only the monoclinic  $m\text{-ZrO}_2$ . Such a difference may be explained by stabilization of the  $t\text{-ZrO}_2$  by oxygen vacancies created in  $m\text{-ZrO}_2$  by interaction with CO.

**Author Contributions:** Conceptualization, writing—original draft preparation, A.V.; methodology, writing—review and editing, A.F. and S.T.; validation, N.S.; formal analysis, N.S.; visualization, investigation, E.M., O.N. and E.K.; data curation, A.L., V.D. and Y.D.; supervision, S.T. and A.F. All authors have read and agreed to the published version of the manuscript.

**Funding:** The work was performed under financial support from the Russian Federation Government Ministry of Science and Higher Education Act No 1.1.1.6 (project No 075-15-2021-1348).

**Data Availability Statement:** All data used to support the findings of this study are available from the corresponding author upon request.

**Acknowledgments:** SEM investigations have been carried out using the equipment of Share Use Centre “Nanotech” of the ISPMS SB RAS.

**Conflicts of Interest:** The authors declare no conflict of interest.

## References

1. Liu, J.; Hao, Z.; Cui, Z.; Ma, D.; Lu, J.; Cui, Y.; Li, C.; Liu, W.; Xie, S.; Hu, P.; et al. Oxidation behavior, thermal stability, and the coating/substrate interface evolution of CrN-coated Zircaloy under high-temperature steam. *Corros. Sci.* **2021**, *185*, 109416. [[CrossRef](#)]
2. Manaud, J.P.; Poulon, A.; Gomez, S.; Petitcorps, Y. Le A comparative study of CrN, ZrN, NbN and TaN layers as cobalt diffusion barriers for CVD diamond deposition on WC–Co tools. *Surf. Coatings Technol.* **2007**, *202*, 222–231. [[CrossRef](#)]
3. Lee, D.B.; Lee, Y.C.; Kwon, S.C. High temperature oxidation of TiCrN coatings deposited on a steel substrate by ion plating. *Surf. Coatings Technol.* **2001**, *141*, 232–239. [[CrossRef](#)]
4. Sidelev, D.V.; Syrtanov, M.S.; Ruchkin, S.E.; Pirozhkov, A.V.; Kashkarov, E.B. Protection of Zr Alloy under High-Temperature Air Oxidation: A Multilayer Coating Approach. *Coatings* **2021**, *11*, 227. [[CrossRef](#)]
5. Gérard, B. Application of thermal spraying in the automobile industry. *Surf. Coatings Technol.* **2006**, *201*, 2028–2031. [[CrossRef](#)]
6. Xia, F.; Xu, H.; Liu, C.; Wang, J.; Ding, J.; Ma, C. Microstructures of Ni–AlN composite coatings prepared by pulse electrodeposition technology. *Appl. Surf. Sci.* **2013**, *271*, 7–11. [[CrossRef](#)]
7. Krysina, O.V.; Ivanov, Y.F.; Koval, N.N.; Prokopenko, N.A.; Shugurov, V.V.; Petrikova, E.A.; Tolkachev, O.S. Composition, structure and properties of Mo–N coatings formed by the method of vacuum-arc plasma-assisted deposition. *Surf. Coatings Technol.* **2021**, *416*, 127153. [[CrossRef](#)]
8. Li, Z.; Liu, C.; Chen, Q.; Yang, J.; Liu, J.; Yang, H.; Zhang, W.; Zhang, R.; He, L.; Long, J.; et al. Microstructure, high-temperature corrosion and steam oxidation properties of Cr/CrN multilayer coatings prepared by magnetron sputtering. *Corros. Sci.* **2021**, *191*, 109755. [[CrossRef](#)]
9. Khamseh, S.; Araghi, H. A study of the oxidation behavior of CrN and CrZrN ceramic thin films prepared in a magnetron sputtering system. *Ceram. Int.* **2016**, *42*, 9988–9994. [[CrossRef](#)]
10. Spitz, S.; Stueber, M.; Leiste, H.; Ulrich, S.; Seifert, H.J. Phase formation and microstructure evolution of reactively r.f. magnetron sputtered Cr–Zr oxynitride thin films. *Surf. Coatings Technol.* **2013**, *237*, 149–157. [[CrossRef](#)]
11. Landälv, L.; Lu, J.; Spitz, S.; Leiste, H.; Ulrich, S.; Johansson-Jöesaar, M.P.; Ahlgren, M.; Göthelid, E.; Alling, B.; Hultman, L.; et al. Structural evolution in reactive RF magnetron sputtered (Cr,Zr)2O3 coatings during annealing. *Acta Mater.* **2017**, *131*, 543–552. [[CrossRef](#)]
12. Mohammadtaheri, M.; Li, Y.; Corona-Gomez, J.; Yang, Q. An investigation on synthesis and characterization of superhard Cr–Zr–O coatings. *Surf. Coatings Technol.* **2019**, *375*, 694–700. [[CrossRef](#)]
13. Kohno, T.; Tanaka, K.; Usui, H.; Lori, O.; Gonen, S.; Elbaz, L.; Shugurov, V.V.; Koval, N.N.; Krysina, O.V.; Prokopenko, N.A. QUINTA equipment for ion-plasma modification of materials and products surface and vacuum arc plasma-assisted deposition of coatings. *J. Phys. Conf. Ser.* **2019**, *1393*, 012131. [[CrossRef](#)]
14. Vorontsov, A.V.; Filippov, A.V.; Shamarin, N.N.; Moskvichev, E.N.; Novitskaya, O.S.; Knyazhev, E.O.; Denisova, Y.A.; Leonov, A.A.; Denisov, V. V Microstructure and residual stresses of ZrN/CrN multilayer coatings produced by the plasma-assisted vacuum-arc method. *Met. Work. Mater. Sci.* **2022**, *24*, 76–89. [[CrossRef](#)]
15. Qi, Z.B.; Wu, Z.T.; Liang, H.F.; Zhang, D.F.; Wang, J.H.; Wang, Z.C. In situ and ex situ studies of microstructure evolution during high-temperature oxidation of ZrN hard coating. *Scr. Mater.* **2015**, *97*, 9–12. [[CrossRef](#)]
16. Harrison, R.W.; Lee, W.E. Mechanism and Kinetics of Oxidation of ZrN Ceramics. *J. Am. Ceram. Soc.* **2015**, *98*, 2205–2213. [[CrossRef](#)]
17. Pilloud, D.; Pierson, J.F.; De Lucas, M.C.M.; Alnot, M. Stabilisation of tetragonal zirconia in oxidised Zr–Si–N nanocomposite coatings. *Appl. Surf. Sci.* **2004**, *229*, 132–139. [[CrossRef](#)]
18. Oettel, H.; Wiedemann, R. Residual stresses in PVD hard coatings. *Surf. Coatings Technol.* **1995**, *76–77*, 265–273. [[CrossRef](#)]
19. David, J.; Trolliard, G.; Gendre, M.; Maître, A. TEM study of the reaction mechanisms involved in the carbothermal reduction of zirconia. *J. Eur. Ceram. Soc.* **2013**, *33*, 165–179. [[CrossRef](#)]
20. Reddy, G.L.N.; Ramana, J.V.; Kumar, S.; Kumar, S.V.; Raju, V.S. Investigations on the oxidation of zirconium nitride films in air by nuclear reaction analysis and backscattering spectrometry. *Appl. Surf. Sci.* **2007**, *253*, 7230–7237. [[CrossRef](#)]
21. Milošev, I.; Strehblow, H.H.; Navinšek, B. Comparison of TiN, ZrN and CrN hard nitride coatings: Electrochemical and thermal oxidation. *Thin Solid Film.* **1997**, *303*, 246–254. [[CrossRef](#)]
22. Panjan, P.; Navinšek, B.; Cvelbar, A.; Zalar, A.; Milošev, I. Oxidation of TiN, ZrN, TiZrN, CrN, TiCrN and TiN/CrN multilayer hard coatings reactively sputtered at low temperature. *Thin Solid Film.* **1996**, *281–282*, 298–301. [[CrossRef](#)]